Effect of angiogenesis inhibition by *Id* loss and the contribution of bone-marrow-derived endothelial cells in spontaneous murine tumors

Marianna B. Ruzinova,[1] Rebecca A. Schoer,[4] William Gerald,[2] James E. Egan,[4] Pier Paolo Pandolfi,[3] Shahin Rafii,[5] Katia Manova,[3] Vivek Mittal,[4,*] and Robert Benezra[1,*]

[1]Program of Cell Biology
[2]Department of Pathology
[3]Program of Molecular Biology
Memorial Sloan-Kettering Cancer Center, New York, New York 10021
[4]Cancer Genome Research Center, Cold Spring Harbor Laboratory, Woodbury, New York 11797
[5]Department of Medicine, Cornell University Medical College, New York, New York 10021
*Correspondence: mittal@cshl.edu (V.M.), r-benezra@ski.mskcc.org (R.B.)

Summary

Angiogenic defects in *Id* mutant mice inhibit the growth of tumor xenografts, providing a genetic model for antiangiogenic stress. Our work tests the consequences of such stress on progression of more physiological *Pten*$^{+/-}$ tumors. While tumor growth occurs despite impaired angiogenesis, disruption of vasculature by *Id* loss causes tumor cells to experience hypoxia and necrosis, the extent of which is tumor dependent. We show that bone-marrow-derived endothelial precursors contribute functionally to neovasculature of some but not all *Pten*$^{+/-}$ tumors, partially rescuing *Id* mutant phenotype. We demonstrate that loss of *Id1* in tumor endothelial cells results in downregulation of several proangiogenic genes, including α*6* and β*4 integrins, matrix metalloprotease-2*, and *fibroblast growth factor receptor-1*. Inhibition of these factors phenocopies loss of *Id* in in vivo angiogenesis assays.

Introduction

Id proteins regulate transcription by sequestering bHLH transcription factors and forming heterodimers that are unable to bind DNA (Ruzinova and Benezra, 2003). *Id1* and *Id3* are required for proper angiogenesis during mouse brain development. Complete loss of these genes leads to aggregation of dilated and irregularly shaped blood vessels and brain hemorrhage by E13.5. Id proteins are also important in tumor angiogenesis. Adult *Id1*$^{+/-}$ *Id3*$^{-/-}$ mice exhibit a block in neovascularization and consequently resist the growth of B6RV2 lymphoma and B-CA breast cancer cells injected subcutaneously. Growth of Lewis lung carcinoma (LLC) xenograft line does occur, but no metastases occur in the *Id* mutant background. In all cases, xenografts grown in *Id1*$^{+/-}$*Id3* $^{-/-}$ animals are hemorrhagic and necrotic with stunted and occluded vasculature (Lyden et al., 1999).

Since xenografts grow subcutaneously, they do not develop in a common site for human tumors and may not be physiologically relevant to human malignancies (Carmeliet and Jain, 2000). Xenograft models may exaggerate antiangiogenic and antitumor responses (Carmeliet and Jain, 2000; Bergers et al., 1999). Thus, we were interested in the role of *Id* genes in the vascularization of spontaneous tumors, which arise from cells in well-vascularized tissues and progress through multiple stages. Since the host organ can affect the biology of the tumor, our goal was to evaluate *Id* mutant vasculature in tumors of different origins. To address this question, we crossed *Id1*$^{-/-}$ *Id3*$^{+/-}$ mice with *Pten*$^{+/-}$ mice. The *Pten* gene encodes a phosphatase homozygously mutated in a high percentage of human tumors. A major substrate of PTEN is phosphatidylinositol triphosphate (PIP-3), a lipid second messenger produced by PI 3-kinase. In the absence of PTEN activity, PIP-3 levels are upregulated, leading to enhanced phosphorylation and activation of the survival-promoting factor Akt/PKB. *Pten*$^{+/-}$ mice exhibit hyperplastic-dysplastic features such as lymph hyperplasia and high tumor incidence, including uterine carcinomas, prostate intraepithelial neoplasias (PINs), and pheochromocytomas (Di Cristofano et al., 1999, 2001).

SIGNIFICANCE

Our work demonstrates that the response of spontaneously arising tumors to severe angiogenic stress is very different from that observed in tumor xenografts. In spontaneous tumors, the consequence of angiogenesis inhibition by *Id* loss varies in severity depending on the tumor type, with some tumors growing to a large size despite hypoxic stress. Spontaneous tumors also show much more variability in their dependence on bone-marrow-derived endothelial precursors than xenografts, which may explain the observed differences in response to *Id* deficiency. We also identify multiple downstream targets of Id1 in endothelial cells of spontaneous tumors, demonstrating that Id regulates several angiogenic pathways in vivo. Overall, our results point to new strategies for the development and use of antiangiogenic drugs.

Loss of *Id* in *Pten*$^{+/-}$ tumors that normally express Id1 and Id3 in the vasculature, such as lymph hyperplasia and uterine carcinoma, results in hemorrhage and necrosis, the extent of which is tumor dependent. No histological changes were found in tumors that do not usually overexpress Id1 in their vasculature, confirming that the observed phenotypes were due to disruption of angiogenesis. While severe angiogenic stress induced by loss of *Id* impaired survival of uterine tumor cells, hyperplastic lymphoid lesions continue to grow to a large size despite the vascular defect. Continued proliferation of hyperplastic lymph cells in the presence of impaired vasculature questions the notion that tumors will not grow past 1–2 mm without oxygen and nutrients delivered by functional vasculature (Carmeliet and Jain, 2000; Kerbel, 2000).

Vascularization of xenografts occurs primarily through recruitment of bone-marrow (BM)-derived circulating endothelial precursors (CEPs). Impaired mobilization of endothelial precursors is responsible for the block in xenograft vascularization and growth in *Id*-deficient mice (Lyden et al., 2001). We demonstrate that *Pten*$^{+/-}$ spontaneous tumors show much more variability in their dependence on BM-derived precursors, with lymph hyperplasias showing no evidence of BM-derived vasculature and uterine carcinomas incorporating BM-derived CEPs into 15%–20% of their neovessels. Importantly, this 15%–20% contribution is functionally significant, since impaired tumor cell survival and increased hemorrhage and necrosis observed in the *Id*-deficient background are partially rescued by wild-type bone marrow transplantation. The difference in incorporation of BM-derived precursors may explain the difference in response of *Pten*$^{+/-}$ spontaneous tumors to *Id*-deficiency, if loss of *Id* partially impairs the integrity of sprouting and co-opted vasculature while completely inhibiting mobilization of CEPs.

Id proteins control lineage determination, differentiation, and proliferation in a number of diverse cell types by regulating transcriptional networks (Ruzinova and Benezra, 2003). Thus, Id proteins' role in angiogenesis may be to regulate the expression of a variety of angiogenic molecules. We used microarray technology to identify angiogenic factors misregulated in *Id1*$^{-/-}$ tumor endothelium. Several proangiogenic genes were downregulated in the *Id1*$^{-/-}$ endothelial cells, including α*6* and β*4 integrins*, *MMP-2*, and *FGFR-1*, as well as members of ephrin and IGF2 families. However, we found no evidence that the angiogenic defect observed in *Id*-deficient tumors is the result of *thrombospondin-1* (*TSP-1*) upregulation, recently reported in *Id1*$^{-/-}$ mouse embryonic fibroblasts (MEFs) (Volpert et al., 2002). In vivo matrigel assays confirmed importance of the identified downstream targets of Id1 in the development of a neovasculature. The finding that these molecules are coordinately regulated by Id1 suggests that inhibiting them in combination may be more effective than inhibiting them separately. In summary, our studies provide a detailed analysis of antiangiogenic stress in spontaneous murine tumors, identify proangiogenic factors regulated by Id1, and point to new strategies for the development and use of antiangiogenic therapy.

Results

Reduction of Id gene dosage does not affect incidence of tumorigenesis in the *Pten*$^{+/-}$ tumor model

After a short latency, 100% of female *Pten*$^{+/-}$ mice develop a severe lymphocytic hyperplasia (DiCristofano et al., 1999). Loss of up to three copies of *Id1* and *Id3* did not reduce the rate of occurrence (Supplemental Figure S1A at http://www.cancercell.org/cgi/content/full/4/4/277/DC1), and loss of two copies of *Id* did not delay the onset of lymphocytic growths (Figure 1A). Loss of three copies of *Id* conferred a slight but statistically significant delay in the onset of lymphadenopathy (Figure 1A).

A high percentage of female *Pten*$^{+/-}$ mice also develop in situ uterine carcinomas (Di Cristofano et al., 2001). Histological examination of *Pten*$^{+/-}$ *Id*-wild-type and *Id* mutant female mice revealed that occurrence of uterine malignancies was not reduced in the absence of *Id* copies (Figure 1B).

Pten$^{+/-}$ mice also develop other tumors such as PINs and pheochromocytomas (Di Cristofano et al., 2001). The incidence of these malignancies was similar in *Id*-wild-type and *Id*-deficient backgrounds (Supplemental Figure S1A). The absence of an effect on the onset of tumors in the *Id* mutant animals is consistent with the finding that expression of *Id* is not detected in these tumor cells but is confined to the tumor vasculature (see below).

Id-deficient lymph and uterine tumors exhibit necrosis and hemorrhage

The hyperplastic lymphoid tissue in *Pten*$^{+/-}$ *Id* wild-type mice has no detectable hemorrhage or necrosis (Figure 1C). In contrast, microscopic hemorrhage and cellular necrosis were commonly observed in *Id* mutant tissue samples (Figure 1D). The extent of tissue damage appeared to be similar in tissues lacking two or three copies of the *Id* genes in various combinations (Supplemental Figures S1B–S1D).

On gross examination, *Pten*$^{+/-}$ uterine carcinomas were rarely hemorrhagic and never exhibited gross necrosis (Figure 1E). In contrast, *Pten*$^{+/-}$*Id1*$^{-/-}$ and *Pten*$^{+/-}$*Id1*$^{-/-}$*Id3*$^{+/-}$ uterine tumors almost always exhibited gross hemorrhage and frequently had extensive necrosis (Figure 1E). Histological examination further confirmed that uterine tumors in *Id* mutant mice were extensively hemorrhagic and necrotic in contrast to uterine carcinomas from *Pten*$^{+/-}$ animals, which were mostly well-differentiated tumors, with only some localized central hemorrhage and necrosis (Figures 1F and 1G). Similar to lymph hyperplasia, the combination of missing *Id1* and/or *Id3* copies did not affect the resulting phenotype (Supplemental Figures S1E–S1G). Quantitative assessment of tumor composition has demonstrated a significant increase in hemorrhage and necrosis and a significant decrease in viable tumor tissue in *Pten*$^{+/-}$ *Id* mutant uterine malignancies as compared to *Pten*$^{+/-}$ *Id* wild-type tumors (Figure 1H). The nonneoplastic uterine wall appeared to be histologically normal (Figures 1F–1G), consistent with the lack of expression of Id1 in normal vasculature (see below). The reduction of *Id* copy number did not impede the very early stages of tumorigenesis, since histological analysis detected dysplastic changes in uterine glands in *Id* mutant animals. Rather, it appears that the reduction of *Id* impairs the growth and/or survival of malignant uterine tissue, causing massive accumulation of necrotic tissue and blood.

The histological appearance of pheochromocytomas and PINs was similar in *Pten*$^{+/-}$ and *Pten*$^{+/-}$ *Id* mutant animals (Supplemental Figures S1H–S1M). The absence of an effect on the histological appearance of these tumors in animals with reduced *Id* dosage is consistent with the observation that Id1 is not overexpressed in the vasculature of these tumors (see below.)

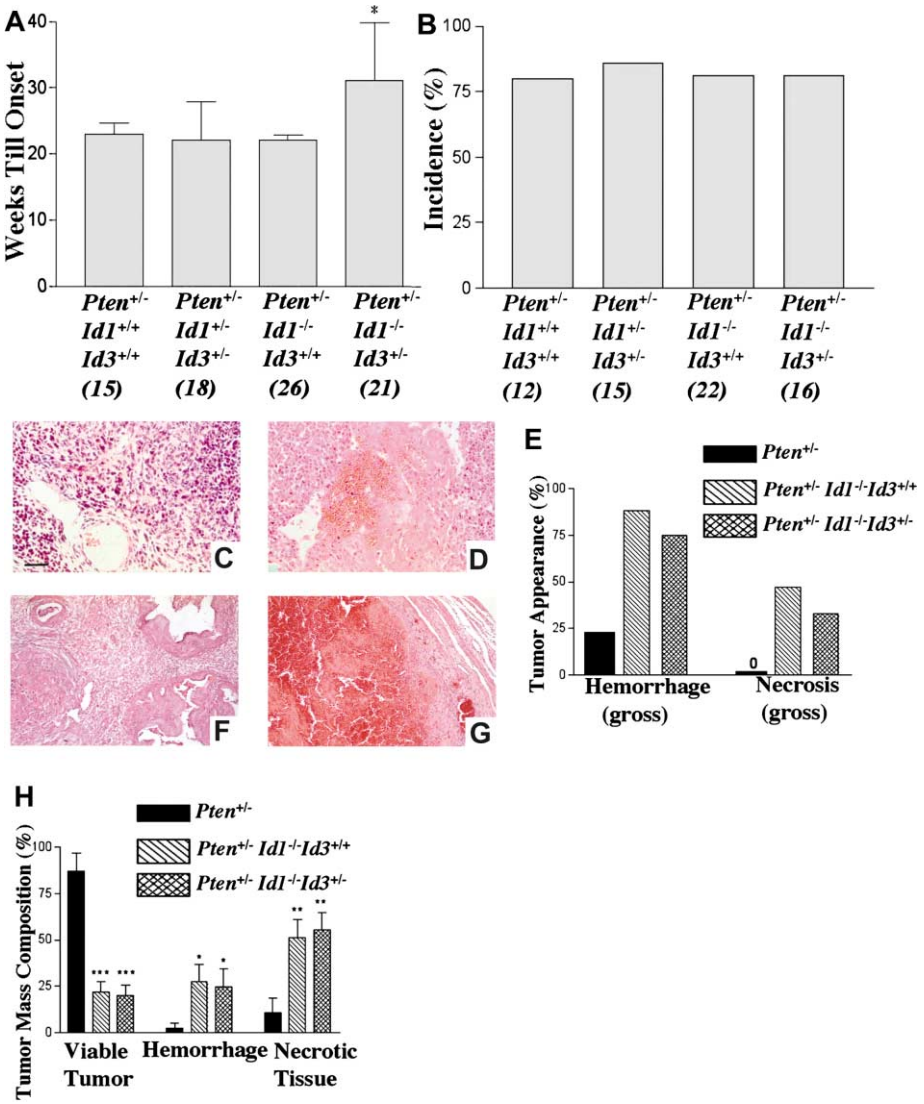

Figure 1. *Id* deficiency impairs tumor cell survival but does not affect tumor incidence or time of onset in *Pten*$^{+/-}$ model

A: Loss of two copies of the *Id* genes does not delay the onset of lymphocytic hyperplasia in *Pten*$^{+/-}$ mice, while the loss of three copies confers a slight but statistically significant delay. Bars show mean age of onset ± SD, and number of mice in each category is given in parentheses.

B: Loss of *Id* genes does not decrease incidence of uterine carcinoma in *Pten*$^{+/-}$ mice. Number of mice in each category is given in parentheses.

C and D: Loss of *Id* causes microscopic hemorrhage and tissue damage in *Pten*$^{+/-}$ lymph hyperplasia. H&E staining reveals (**C**) intact tissue in *Pten*$^{+/-}$ (n = 10) and (**D**) microscopic hemorrhage in *Pten*$^{+/-}$*Id1*$^{-/-}$ lymph hyperplasia (n = 10).

E: Gross examination reveals occasional hemorrhage and absence of visible necrosis in *Pten*$^{+/-}$ uterine carcinomas (n = 9), while frequent gross hemorrhage and necrosis are observed in *Pten*$^{+/-}$ *Id1*$^{-/-}$ (n = 17) and *Pten*$^{+/-}$ *Id1*$^{-/-}$*Id3*$^{+/-}$ (n = 12) uterine tumors.

F and G: Loss of *Id* drastically affects tumor cell survival in *Pten*$^{+/-}$ uterine carcinoma. Histological analysis detected (**F**) viable tissue in *Pten*$^{+/-}$ *Id*-wild-type animals (n = 9), while most sections from *Pten*$^{+/-}$ *Id1*$^{-/-}$ animals contained (**G**) hemorrhage and necrosis (n = 10). No tissue damage was detected in *Pten*$^{+/-}$ *Id1*$^{-/-}$ nonneoplastic uterine wall.

H: Quantitation of uterine tumor composition demonstrates statistically significant reduction of viable tumor tissue and increase in hemorrhage and necrosis in *Pten*$^{+/-}$ *Id1*$^{-/-}$ (n = 10) and *Pten*$^{+/-}$ *Id1*$^{-/-}$*Id3*$^{+/-}$ (n = 10) uterine tumors as compared to *Pten*$^{+/-}$ uterine malignancies (n = 9).

Scale bar, 25 μm (**C and D**); 100 μm (**E and F**).

Expression of Id1 and Id3 is confined to tumor endothelial cells

Changes in the appearance of the lymph and uterine malignancies in *Id*-deficient mice led us to investigate whether these effects were due to the reduction of *Id* gene expression in tumor cells or endothelial cells. In situ and immunohistochemistry experiments, including staining of adjacent sections with endothelial marker CD31, demonstrated that expression of both *Id1* mRNA and Id1 protein were confined exclusively to the vasculature of hyperplastic lymph nodes of *Pten*$^{+/-}$ animals (Figures 2A–2C). *Id3* mRNA expression was also localized in blood vessels, although very low background levels of expression were also detected in lymphocytic cells (Figure 2D). Analysis of *Pten*$^{+/-}$ uterine carcinomas revealed that expression of Id1 protein and *Id3* mRNA were also confined to endothelial cells (Figures 2E–2H). In contrast, expression of Id1 protein and *Id3* mRNA was virtually undetectable in endothelial cells of the unaffected uterine wall (Figures 2G–2J). Interestingly, expression of Id1 was weak or undetectable in malignancies devoid of necrosis or hemorrhage in the *Id*-deficient background, such as PINs and pheochromocytomas (Supplemental Figures S2A and S2B). Thus, the increase in hemorrhage and necrosis observed in the lymph hyperplasias and uterine tumors is likely due to defects in the vasculature within these tumors.

Upregulation of *Id* gene expression may also play a role in human tumor angiogenesis. Previous studies detected *Id1* and *Id3* mRNA expression in endothelial cells of high-grade human glial tumors (Lyden et al., 1999; Vandeputte et al., 2002). Immunohistochemistry has confirmed Id1 upregulation in endothelial cells of a variety of other human malignancies, including endometrial and lymphoid tumors (Figures 2K and 2L), as well as lung, stomach, large bowel, kidney, and ovarian adenocarcinomas (Supplemental Figures S2C–S2I).

Tumor vasculature in the *Id* mutant background is morphologically abnormal and functionally impaired

CD31 immunohistochemistry of *Pten*$^{+/-}$ hyperplastic lymphoid tissue revealed numerous fine capillaries (Figure 3A). In contrast, staining of *Pten*$^{+/-}$ *Id* mutant lymph hyperplasia with CD31 revealed anastomosing networks of enlarged, dilated, and irregu-

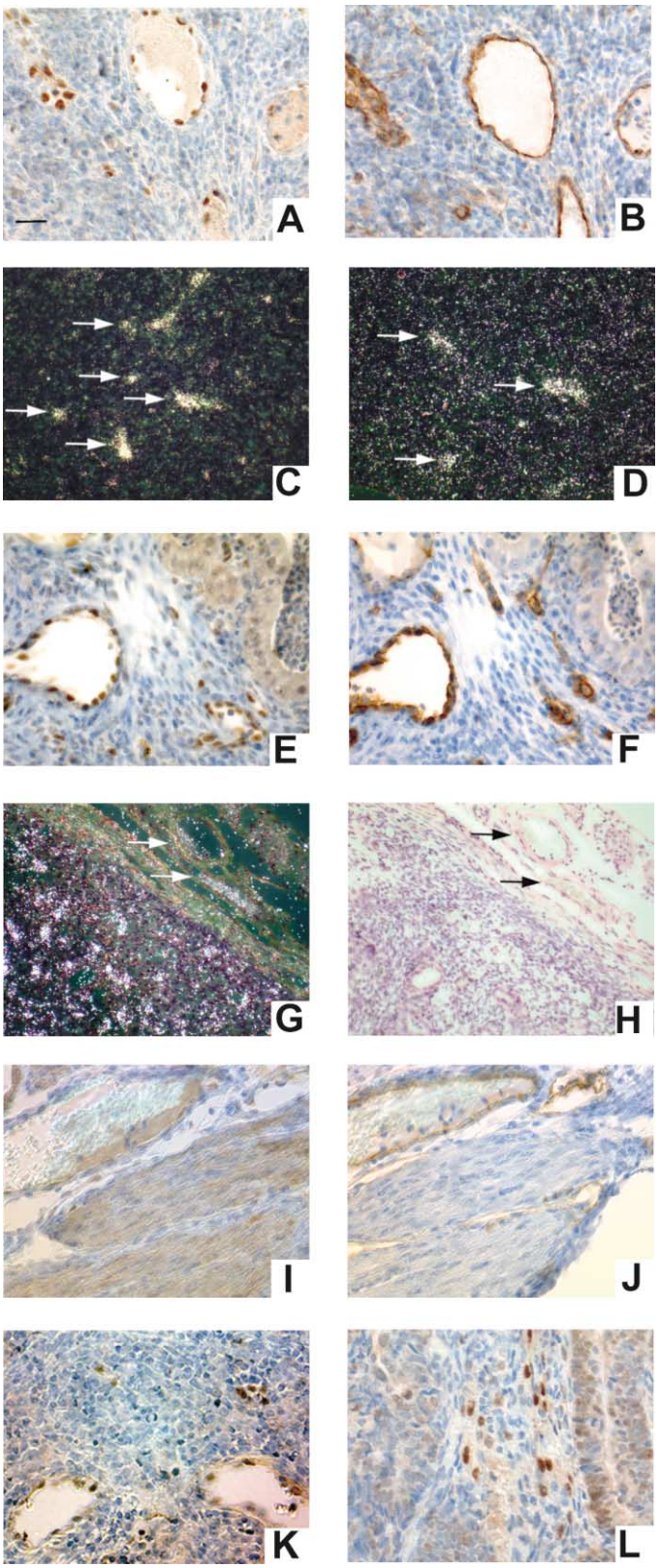

Figure 2. Expression of *Id* genes is confined to tumor vasculature

A, E, and I: Id1 staining of *Pten*$^{+/-}$ (**A**) lymph hyperplasia (n = 8), (**E**) uterine carcinoma (n = 6), and (**I**) nonneoplastic uterine wall (n = 6).
B, F, and J: CD31 staining of adjacent sections of *Pten*$^{+/-}$ (**B**) lymph hyperplasia (n = 8), (**F**) uterine carcinoma (n = 6), and (**J**) nonneoplastic uterine wall (n = 6).
C and D: *Id1* (n = 6) and *Id3* (n = 4) expression, respectively, in Pten$^{+/-}$ lymphocytic hyperplasia. Arrows point to blood vessels.
G and H: *Id3* expression in blood vessels of *Pten*$^{+/-}$ uterine carcinoma and uterine wall (n = 6), dark and light field, respectively. Arrows point to *Id3*-negative blood vessels of uterine wall.
K and L: Id1 expression in blood vessels of human lymphomas (6/7) and endometrial adenocarcinomas (3/3), respectively.
Scale bar, 25 μm (**A, B, E, F, and I–L**); 50 μm (**C, D, and G–H**).

larly shaped blood vessels (Figure 3B). There was a significant increase in vascular density in tumors grown in the *Id* mutant background as compared to wild-type (Figure 3C). The vascular phenotype found in tumor tissue was very similar to that described in the brain of *Id*$^{-/-}$*Id3*$^{-/-}$ embryos. However, it differed from the stunted vasculature found in xenografts of *Id*-deficient mice. The extent of vascular malformation appeared to be similar in tissues lacking two or three copies of the *Id* genes in different combinations (Supplemental Figures S3A–S3C).

Uterine carcinomas in *Pten*$^{+/-}$ animals are well-vascularized malignancies (Figure 3D). The extreme damage to uterine carcinoma tissue observed in the *Id*-deficient background hampered detailed analysis of vascular markers. However, in a few cases of uterine carcinoma in *Pten*$^{+/-}$ *Id1*$^{-/-}$ *Id3*$^{+/+}$ mice with viable tumor tissue still detectable, vascular malformations very similar to those found in lymph hyperplasia and *Id1*$^{-/-}$*Id3*$^{-/-}$ embryos could be seen (Figure 3E). Areas of extensive necrosis surrounded malformed vasculature (Figure 3F). The normally *Id*-negative vasculature in the intact uterine wall appeared normal (Figure 3G).

Immunodetection of hypoxia-inducible factor 1α (HIF-1α), a primary regulator of hypoxia-inducible genes (Harris, 2002), provided evidence that morphologically abnormal *Id* mutant vasculature is also functionally impaired. Normally, mammalian cells are localized within 100–200 μm of blood vessels because they require oxygen and nutrients for their survival (Harris, 2002; Carmeliet and Jain, 2000). In agreement with this observation, hypoxic cells in *Pten*$^{+/-}$ animals with intact *Id* alleles were localized several cells away from blood vessels as revealed by staining adjacent sections with CD31 (Figures 3H and 3I). In contrast, large numbers of hypoxic cells were present in the immediate vicinity of *Id* mutant blood vessels despite the increased vascular density (Figures 3J and 3K).

In order to further characterize *Id* mutant vasculature, we used high molecular weight fluorescent dextran to compare the vascular permeability of tumor vasculature in the *Id*-wild-type and mutant background. Reduction of *Id* gene expression causes increased vascular permeability in the lymphocytic hyperplasias (Figures 3L and 3M).

Contribution of BM-derived CEPs to neovasculature of *Pten*$^{+/-}$ tumors

Previous work has shown that vascularization of xenografts relies predominantly on CEPs, mobilization of which is impaired in the *Id*-deficient background. Bone marrow transplantation from a wild-type donor restores angiogenesis in xenografts of *Id* mutant mice. Incorporation of BM-derived, vascular endothelial growth factor receptor 2-positive (VEGFR2^{+}) CEPs was seen in close to 100% of xenograft neovessels, which were also surrounded by donor-derived VEGFR-1^{+} myeloid cells. Mobilization and incorporation of BM CEPs was not a result of bone

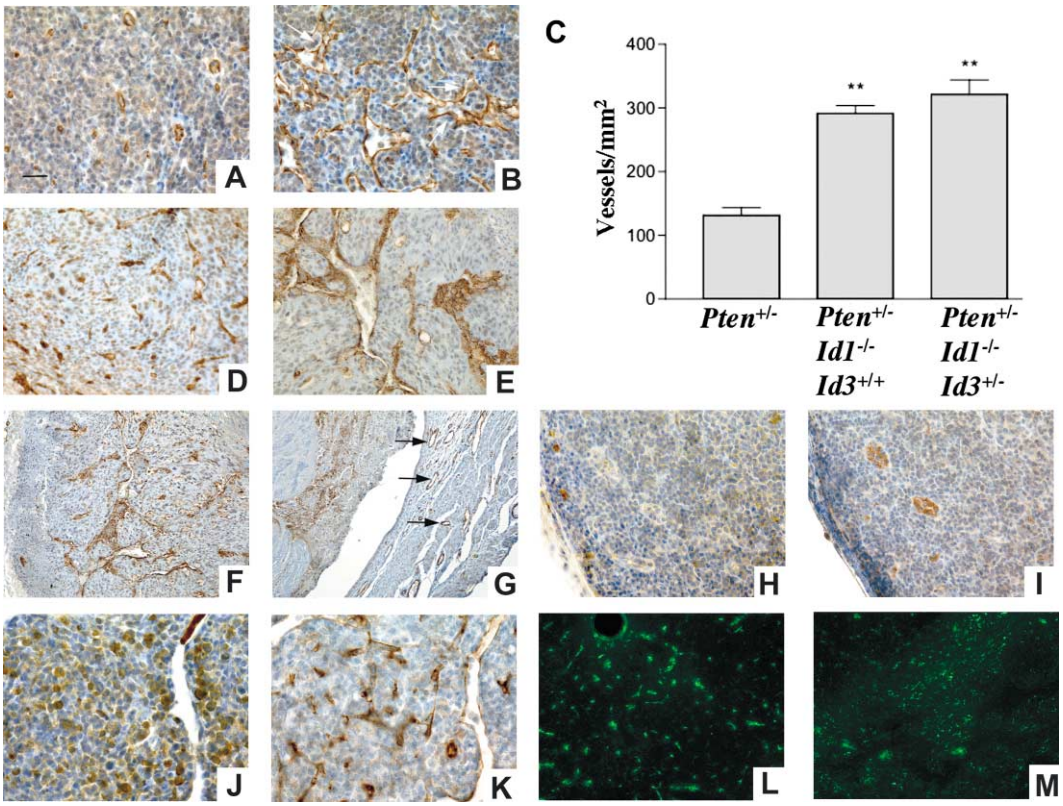

Figure 3. Tumor vasculature in the *Id* mutant background is morphologically abnormal and functionally deficient

A, B, D, and E: CD31 staining highlights normal blood vessels in $Pten^{+/-}$ (**A**) lymph hyperplasia (n = 8) and (**D**) uterine carcinoma (n = 6) and dilated mutant blood vessels in $Pten^{+/-}Id1^{-/-}$ (**B**) lymph hyperplasia (n = 8) and (**E**) uterine carcinoma (n = 3). Arrows point to dilated anastomosing vessels in *Id* mutant lymph hyperplasia.

C: Microvessel density in $Pten^{+/-}$ $Id1^{-/-}$ (n = 5) and $Pten^{+/-}$ $Id1^{-/-}Id3^{+/-}$ (n = 5) lymph hyperplasias was significantly higher than microvessel density in $Pten^{+/-}$ (n = 5) lymph hyperplasias.

F and G: Loss of the *Id1* gene affects cell survival only where it is normally expressed in vasculature. In $Pten^{+/-}$ $Id1^{-/-}$ uterine carcinoma, (**F**) areas with mutant vasculature are surrounded by areas of extensive necrosis, while (**G**) nonneoplastic uterine wall remains unaffected and has morphologically normal vasculature. Arrows point to morphologically normal blood vessels in the uterine wall.

H–K: Oxygen delivery is impaired in lymph hyperplasia with mutant vasculature, causing tumor cells to become hypoxic. HIF1α (**H and J**) and CD31 (**I and K**) staining of adjacent sections reveals that in (**H and I**) $Pten^{+/-}$ *Id*-wild-type lymph hyperplasia, hypoxic cells are located at a considerable distance from blood vessels (n = 5), while in (**J and K**) $Pten^{+/-}$ $Id1^{-/-}$ lymph hyperplasia, increased numbers of hypoxic cells are clustered in close proximity to vessels (n = 5).

L and M: Loss of *Id1* increases permeability of tumor vasculature. Injection of high MW fluorescent dextran demonstrates the increased permeability to this molecule in *Id1* mutant tissue, as evidenced by (**L**) the vessel-associated staining in $Pten^{+/-}$ *Id*-wild-type lymph hyperplasia (n = 4) when compared to (**M**) diffuse staining in $Pten^{+/-}$ $Id1^{-/-}$ lymph tumors (n = 4).

Scale bar, 25 μm (**A, B, D, E, and H–M**); 100 μm (**F and G**);

marrow transplantation per se, since bone marrow transplantation from an *Id* mutant donor fails to restore angiogenesis in *Id* mutant mice (Lyden et al., 2001).

Given the significant differences between the behavior of xenografts and $Pten^{+/-}$ tumors in the *Id* mutant background, we were interested in investigating the origin of vasculature in spontaneously arising tumors. Lethally irradiated $Pten^{+/-}$ and $Pten^{+/-}$ $Id1^{-/-}Id3^{+/-}$ mice were reconstituted with bone marrow from Rosa 26 mice expressing a β-gal transgene in all of their tissues. Lymph hyperplasias and uterine carcinomas developing in these animals were analyzed for incorporation of $LacZ^+$ cells into neovasculature and presence of $VEGFR1^+$ $LacZ^+$ and $VEGFR2^+LacZ^+$ cells.

No appreciable incorporation of $LacZ^+$ cells was seen in vasculature of lymph hyperplasias from either $Pten^{+/-}$ or $Pten^{+/-}$ $Id1^{-/-}Id3^{+/-}$ animals (Figures 4A and 4B). In contrast, $LacZ^+$ cells were detected in blood vessels of uterine carcinomas from both $Pten^{+/-}$ and $Pten^{+/-}$ $Id1^{-/-}Id3^{+/-}$ animals (Figures 4C and 4D). In order to confirm that BM-derived $LacZ^+$ cells were giving rise to endothelial cells, we performed staining with CD31 and observed that some of the CD31 cells were also $LacZ^+$ (Figure 4E). On average, 16% and 16.5% of CD31-positive vessels were $LacZ^+$ in $Pten^{+/-}$ and $Pten^{+/-}$ $Id1^{-/-}Id3^{+/-}$ animals, respectively (Figure 4G). Other $LacZ^+$ cells were observed to be negative for CD31 and localized in the immediate vicinity of blood vessels (Figure 4F). Since BM-derived xenograft vasculature was associated with $LacZ^+VEGFR1^+$ myeloid cells (Lyden et al., 2001), we performed staining with this marker and observed that $LacZ^+$ cells associated with vasculature in uterine tumors were also positive for VEGFR1 (Figures 4H and 4I). $LacZ^+$ vessels were

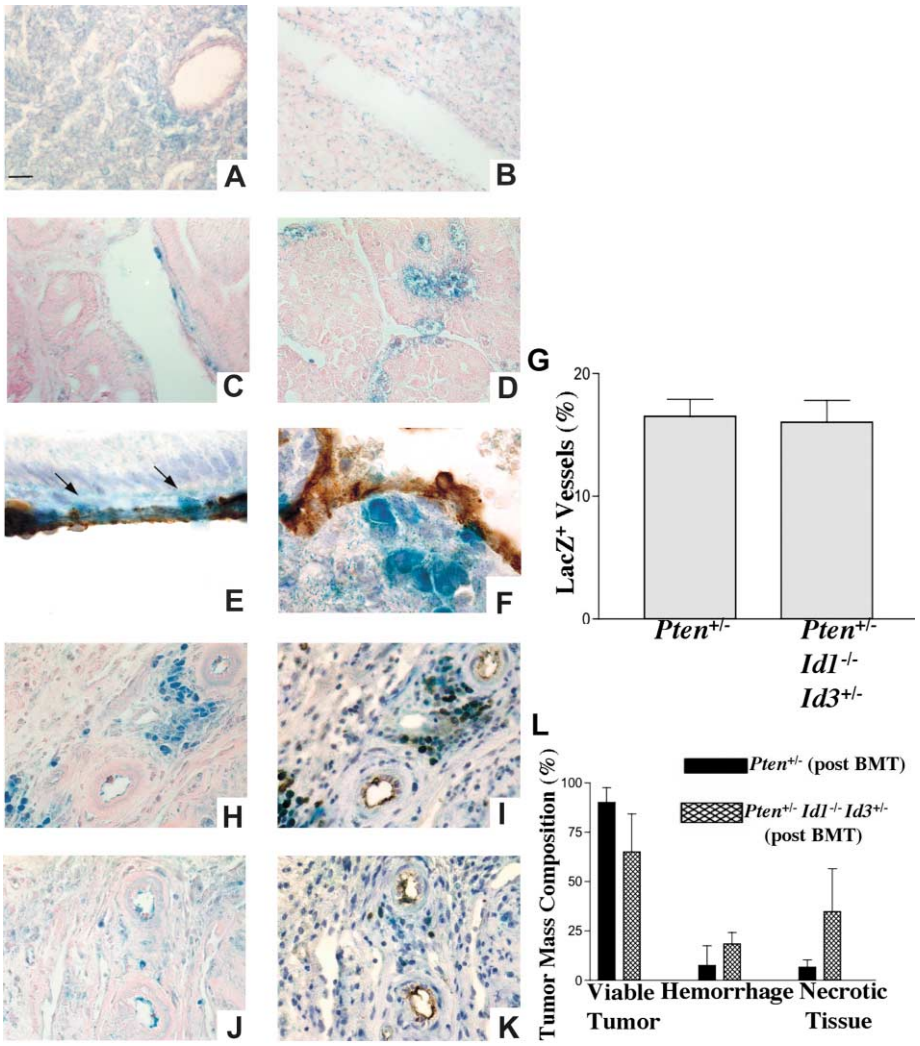

Figure 4. Contribution of BM-derived CEPs to neovasculature of *Pten*$^{+/-}$ tumors

A and B: No LacZ^{+} blood vessels were detected in either (**A**) *Pten*$^{+/-}$ (n = 5) or (**B**) *Pten*$^{+/-}$ *Id1*$^{-/-}$ *Id3*$^{+/-}$ (n = 8) lymph hyperplasias post bone marrow transplant from Rosa 26 mice.

C and D: Under the same conditions, incorporation of LacZ^{+} cells was seen in both (**C**) *Pten*$^{+/-}$ (n = 5) and (**D**) *Pten*$^{+/-}$ *Id1*$^{-/-}$ *Id3*$^{+/-}$ (n = 8) uterine carcinoma tumors.

E: Incorporation of LacZ^{+} cells into blood vessels was verified by counterstaining LacZ^{+} cells with CD31 (n = 13). Arrows point to the LacZ^{+} cells that also stain for CD31.

F: Numerous LacZ^{+} but CD31-negative cells were also observed to closely associate with blood vessels (n = 13).

G: 16.5% and 16% of CD31-positive blood vessels were observed to incorporate LacZ^{+} endothelial cells in *Pten*$^{+/-}$ (n = 5) and *Pten*$^{+/-}$ *Id1*$^{-/-}$ *Id3*$^{+/-}$ (n = 8) uterine carcinomas, respectively.

H and I: Staining adjacent sections with (**I**) VEGFR1 demonstrated that the majority of (**H**) LacZ^{+} cells in close proximity of blood vessels are VEGFR1^{+} (n = 13).

J and K: Staining of adjacent sections with (**K**) VEGFR2 revealed that (**J**) LacZ^{+} cells in blood vessels are VEGFR2^{+}.

L: Quantitation of uterine tumors' composition revealed that percentage of viable tumor, hemorrhage, and necrosis found in *Pten*$^{+/-}$ (n = 5) and *Pten*$^{+/-}$ *Id1*$^{-/-}$*Id3*$^{+/-}$ (n = 8) post bone marrow transplantation were no longer significantly different from each other.

Scale bar, 25 μm (**A–D and H–K**) 10 μm (**E and F**).

seen to express both VEGFR1 and VEGFR2 (Figures 4H–4K). Incorporation of LacZ^{+}VEGFR2^{+} cells into blood vessels provides evidence that BM-derived CEPs are capable of contributing to spontaneous tumor neoangiogenesis. LacZ^{+}VEGFR2^{+} cells were also occasionally seen around vessels, possibly representing migrating CEPs (Figures 4J and 4K).

Since BM-derived CEPs and myeloid cells restored angiogenesis and tumor growth in xenografts of *Id* mutant mice (Lyden et al., 2001), we evaluated whether bone marrow transplant reduced hemorrhage and necrosis in *Pten*$^{+/-}$ *Id1*$^{-/-}$*Id3*$^{+/-}$ mice. Quantitation of tumor composition in *Pten*$^{+/-}$ *Id1*$^{-/-}$*Id3*$^{+/-}$ mice reconstituted with LacZ^{+} wild-type bone marrow indicated that the presence of BM-derived CEPs dramatically increased viable tumor tissue and reduced hemorrhage and necrosis as compared to untransplanted *Pten*$^{+/-}$ *Id1*$^{-/-}$*Id3*$^{+/-}$ mice (Figure 4L and 1H). *Pten*$^{+/-}$ *Id1*$^{-/-}$*Id3*$^{+/-}$animals still exhibited more hemorrhage and necrosis and less viable tumor tissue than *Pten*$^{+/-}$ mice, but these measurements were no longer significantly different in *Id*-wild-type and mutant mice (Figure 4L and 1H). Our results demonstrate that BM-derived CEPs have a functional role in angiogenesis of some but not all spontaneously arising tumors in *Pten*$^{+/-}$ mice.

Id1 regulates several proangiogenic surface proteins

The fact that *Id* genes control the expression of other genes prompted us to use DNA microarrays to evaluate differences in gene expression between *Id*-wild-type and mutant tissues. Initial experiments utilized whole tumor tissue since Id1 is expressed exclusively in the tumor vasculature, and thus detected changes in expression would, at least partially, reflect the changes in endothelial cells. We chose to compare gene expression in hyperplastic lymphoid tissue from *Pten*$^{+/-}$ *Id1*$^{+/+}$ and *Pten*$^{+/-}$ *Id1*$^{-/-}$ mice, since the extensive hemorrhage and necrosis present in uterine carcinoma prevented rigorous analysis.

Hierarchical clustering analysis (Eisen et al., 1998) was used on the filtered data set to visualize genes showing consistent expression profiles across individual experiments (Figure 5A). We mainly focused on genes that were previously known to be involved in angiogenesis and whose expression was downregulated in *Id1* mutant samples. We reasoned that such genes would be potential targets for antiangiogenic therapy. The following genes met these criteria: β*4 integrin*, α*6 integrin, fibroblast growth factor receptor-1 (FGFR1)*, and *metalloprotease-2 (MMP-2)*. We confirmed the array data using semiquantitative PCR (Figure 5B). We also detected further downregulation of

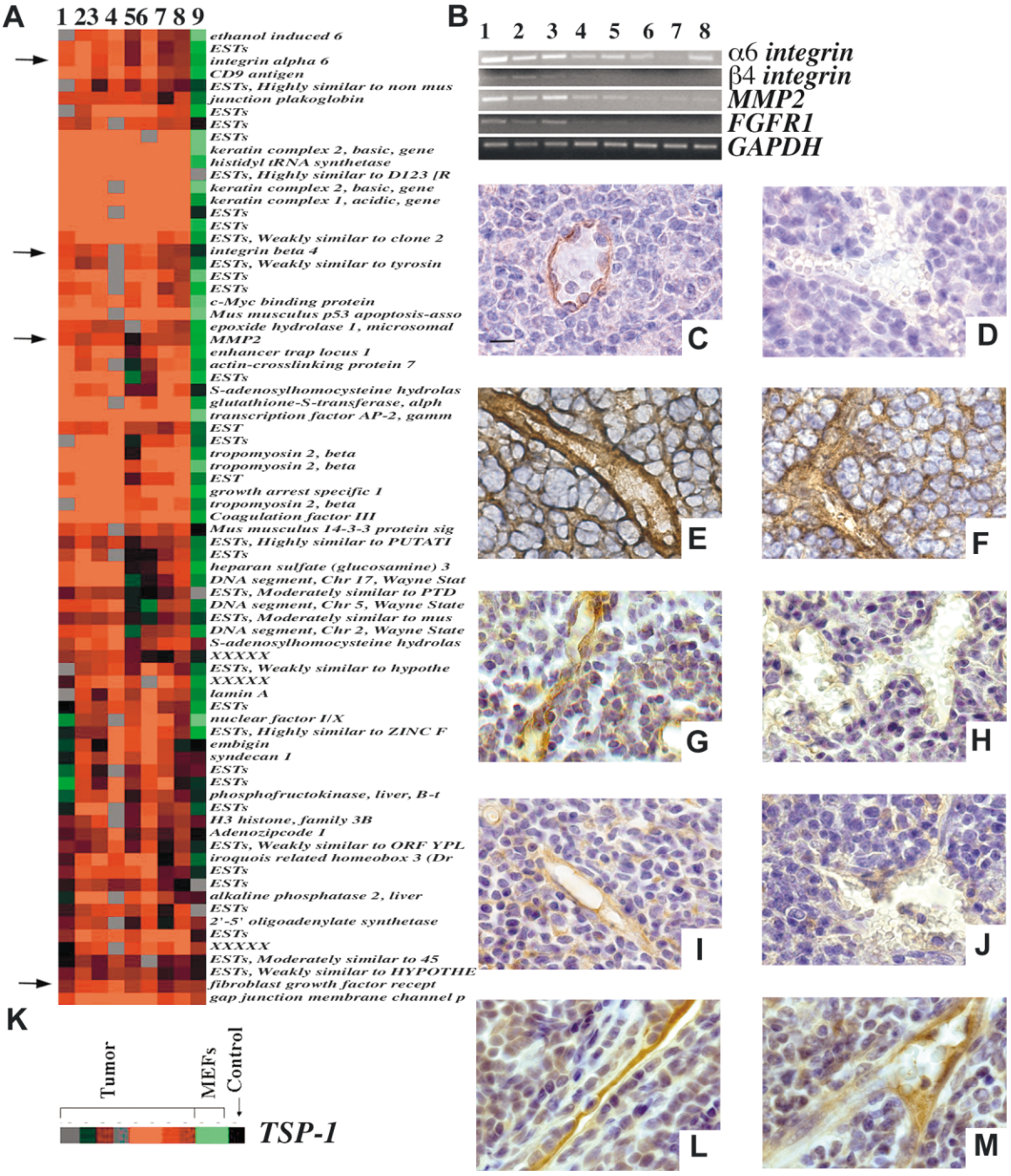

Figure 5. Downstream targets of Id1 in tumor angiogenesis

A: Genes were clustered to show consistency in independent *Pten*$^{+/-}$ *Id1*$^{+/+}$ versus *Pten*$^{+/-}$*Id1*$^{-/-}$ experimental comparisons (columns 1–8). As an example, the expanded view of a downregulated gene cluster in *Pten*$^{+/-}$ *Id*$^{-/-}$ mice is shown. Each column represents data from one comparison and each row is a gene on the array. The last column (9) is a control (*Pten*$^{+/-}$ lymph hyperplasia versus normal lymph tissue). Arrows indicate genes used for further analysis. Red: upregulation in *Pten*$^{+/-}$/downregulation in *Pten*$^{+/-}$*Id1*$^{-/-}$ tissue, green: downregulation in *Pten*$^{+/-}$/upregulation in *Pten*$^{+/-}$*Id1*$^{-/-}$ tissue; black: no change; gray: missing values.

B: Confirmation of microarray results. Semiquantitative RT-PCR was carried out on mRNA samples obtained from *Pten*$^{+/-}$*Id*-wild-type mice (lanes 1–3), *Pten*$^{+/-}$ *Id1*$^{-/-}$ *Id3*$^{+/+}$ mice (lanes 4–6), and *Pten*$^{+/-}$*Id1*$^{-/-}$*Id3*$^{+/-}$ mice (lanes 7–8).

C–J: Staining with (**C and D**) β4 integrin, (**E and F**) α6 integrin, (**G and H**) MMP-2, and (**I and J**) FGFR-1 in (**C**, **E**, **G**, and **I**) *Pten*$^{+/-}$ *Id*-wild-type (n = 5) and (**D**, **F**, **H**, **and I**) *Pten*$^{+/-}$ *Id1*$^{-/-}$ (n = 5) lymphocytic hyperplasia.

K: Results of experimental hybridizations did not detect upregulation of *TSP-1* in *Pten*$^{+/-}$ *Id1*$^{-/-}$ hyperplastic lymph tissue, even though upregulation was observed in *Id1*$^{-/-}$ *Id3* $^{-/-}$ MEFs when compared to wild-type MEFs.

L and M: Staining with TSP 1 did not reveal difference in expression between (L) *Pten*$^{+/-}$ *Id*-wild-type (n = 4) and (M) *Pten*$^{+/-}$ *Id1*$^{-/-}$ (n = 4) lymph hyperplasia. Scale bar, 10 μm (**C–J**, **L, and M**).

MMP-2 and *FGFR-1* levels in the *Id1*$^{-/-}$*Id3*$^{+/-}$ background relative to *Id1*$^{-/-}$*Id3*$^{+/+}$ (Figure 5B), suggesting that *Id3* may regulate these factors as well.

Immunohistochemistry revealed that β4 integrin localized exclusively to endothelial cells (Figure 5C). In agreement with the microarray results, *Pten*$^{+/-}$ tissue expressed higher levels of this molecule than *Pten*$^{+/-}$ *Id1*$^{-/-}$ tissue, where expression was very weak (Figure 5D, Supplemental Figure S3D). Immunohistochemistry also showed that the α6 integrin subunit localized exclusively to endothelial cells (Figure 5E). However, no obvious difference in staining intensity of α6 integrin was detected in the *Id1* mutant background (Figure 5F). The change in expression, confirmed by RT-PCR, is most likely below the sensitivity of immunohistochemical detection.

Microarray analysis also showed consistent downregulation of *FGFR-1* and *MMP-2* in *Pten*$^{+/-}$ *Id1*$^{-/-}$ tissue (Figures 5A and 5B). Both FGFR-1 and MMP-2 are important regulators of tumor angiogenesis (Powers et al., 2000; Haas and Madri, 1999), and both are expressed in endothelial cells in *Pten*$^{+/-}$ tissue (Figures 5G and 5I). We also detected diminished expression of these molecules by immunohistochemistry in the *Pten*$^{+/-}$*Id1*$^{-/-}$ blood vessels (Figures 5H and 5J, Supplemental Figure S3D).

To further confirm that downregulation of identified angiogenic factors in *Id1*$^{-/-}$ tissue is specific to endothelial cells, we isolated endothelial cells from *Id1*$^{+/+}$ and *Id1*$^{-/-}$ lymph hyperplasias by modifying a previously published protocol (St Croix et al., 2000) (Figure 6A). The purity of isolated endothelial cells was 90%–95% as assessed by immunofluorescence with CD31 and von Willebrand factor (Figures 6B–6E). RT-PCR analysis revealed that *Id1*$^{-/-}$ endothelial cells expressed diminished levels of α*6* and β*4 integrins, MMP-2*, and *FGFR1* (Figure 6F), validating results of the initial analysis performed on whole tumor tissue.

T7-based linear amplification of RNA obtained from *Id1*-wild-type and -mutant endothelial cells allowed us to carry out additional microarray experiments, which again confirmed downregulation of *FGFR1*, *MMP-2*, α*6*, and β*4 integrins* in *Id1*$^{-/-}$ endothelium (Table 1). We also found that a number of other angiogenesis-related genes were downregulated 2- to 6-fold in the *Id1*$^{-/-}$ background, such as members of ephrin, the insulin-like growth factor 2 (IGF2), and transforming growth factor β (TGFβ) families, as well as genes encoding extracellular matrix (ECM) proteins and cell adhesion factors (Table 1). In addition, 6-fold upregulation of *Hif1*α was detected in *Id1*$^{-/-}$ endothelial cells (Table 1).

A recent study reported upregulation of TSP-1 in *Id1*$^{-/-}$ MEFs, and elevated levels of TSP-1 have been proposed to account for the angiogenic defect in *Id1* mutant mice (Volpert et al., 2002). Our experiments with *Id*-wild-type and *Id1*$^{-/-}$*Id3*$^{-/-}$ MEFs confirmed the findings by Volpert et al. in that experimental system (Figure 5K). However, we were unable to find consistent upregulation of *TSP-1* in *Id1*$^{-/-}$ spontaneously arising tumors (Figure 5K). No upregulation of *TSP-1* was seen in the purified *Id1*$^{-/-}$ endothelial cells by either RT-PCR or array analysis (Figure 6F, data not shown). Immunohistochemistry also failed to detect upregulation of TSP-1 in tumor cells, tumor stroma, or tumor endothelial cells grown in *Id1*$^{-/-}$ background (Figures 5L and 5M). Thus, upregulation of TSP-1 cannot explain the angiogenic defect seen in *Pten*$^{+/-}$*Id1*$^{-/-}$ tumors.

Functional validation of the downstream targets

We used in vivo matrigel assays to establish whether loss of function, either separately or in combination, of α6β4 integrins, FGFR-1, and MMP-2 is sufficient to account for the angiogenic defects in *Id* mutant mice. Analysis of VEGF-impregnated matrigel plugs from wild-type animals revealed multiple channels created by endothelial cells (Figure 7A). Matrigel-plug-implanted *Id1*$^{-/-}$*Id3*$^{+/-}$ animals fail to form endothelial tubes (Lyden et al., 2001), and the numbers of invading endothelial cells are low and mostly confined to the periphery of the plugs (Figure 7B).

When a blocking antibody to α6 integrin (Zent et al., 2001) was added to matrigel injected into wild-type mice, a partial phenocopy of *Id* mutant angiogenic defect was seen. Endothelial cells failed to form luminized channels, but the numbers of invading endothelial cells were greater than those seen in the matrigel plugs of *Id* mutant mice. An isotype-matched control antibody did not inhibit formation of luminized vessels (Figures 7C and 7D).

The antiangiogenic phenotype associated with inhibition of the α6 integrin subunit may be due to the blockade of α6β1 integrin rather than α6β4. However, our microarray results suggest that the defect involves downregulation of α*6*β*4* rather than α*6*β*1 integrin* since α*6* and β*4 integrins* exhibited consistent downregulation in *Id1*$^{-/-}$ tissue in multiple independent experiments, whereas the levels of β*1* fluctuated.

We also tested a blocking antibody to FGF receptors (Meitinger et al., 2001), which primarily interferes with FGFR-1, in the matrigel assay. Neutralizing FGFR1 inhibited endothelial tube formation and resulted in decreased numbers of invading endothelial cells, producing a phenotype very similar to that of *Id1*$^{-/-}$*Id3*$^{+/-}$ mice. Addition of control antibody to matrigel did not inhibit tube formation (Figures 7E and 7F).

Peptide gelatinase inhibitor, which preferentially targets MMP-2 (Koivunen et al., 1999), was used to block MMP-2 function in the matrigel assay. The resulting phenotype was more severe than that seen with α6 and FGFR-1 blocking antibodies. Virtually no endothelial cells were seen to invade the matrigel plugs, with the majority localized at the edge of the implant. Matrigel plugs impregnated with vehicle alone formed endothelial tubes (Figures 7G and 7H). Decreased levels of MMP-2 may therefore account for the decreased numbers of the invading endothelial cells seen in matrigel plugs of *Id* mutant animals.

Thus, we demonstrate that combined downregulation of MMP-2 and FGFR-1 may account for the reduced endothelial cell invasion and tube formation seen in *Id*-deficient mice. We demonstrate that α6 integrin also plays a role in endothelial tube formation, with its effect likely to be due to a reduction in a α6β4 integrin levels.

Discussion

In this study, we investigate the consequences of reduced expression of *Id1* and *Id3* genes on the development and progression of spontaneously arising malignancies in the *Pten*$^{+/-}$ murine tumor model. We report that deficiency of *Id* genes in tumor endothelial cells, where they are usually expressed, causes formation of anastomosing and dilated blood vessels that exhibit increased vascular permeability. The function of malformed tumor vasculature in *Id* mutant mice was impaired, since tumor cells located in close proximity to these vessels experience hypoxia. Chronic hypoxia impairs cell survival (Harris, 2002),

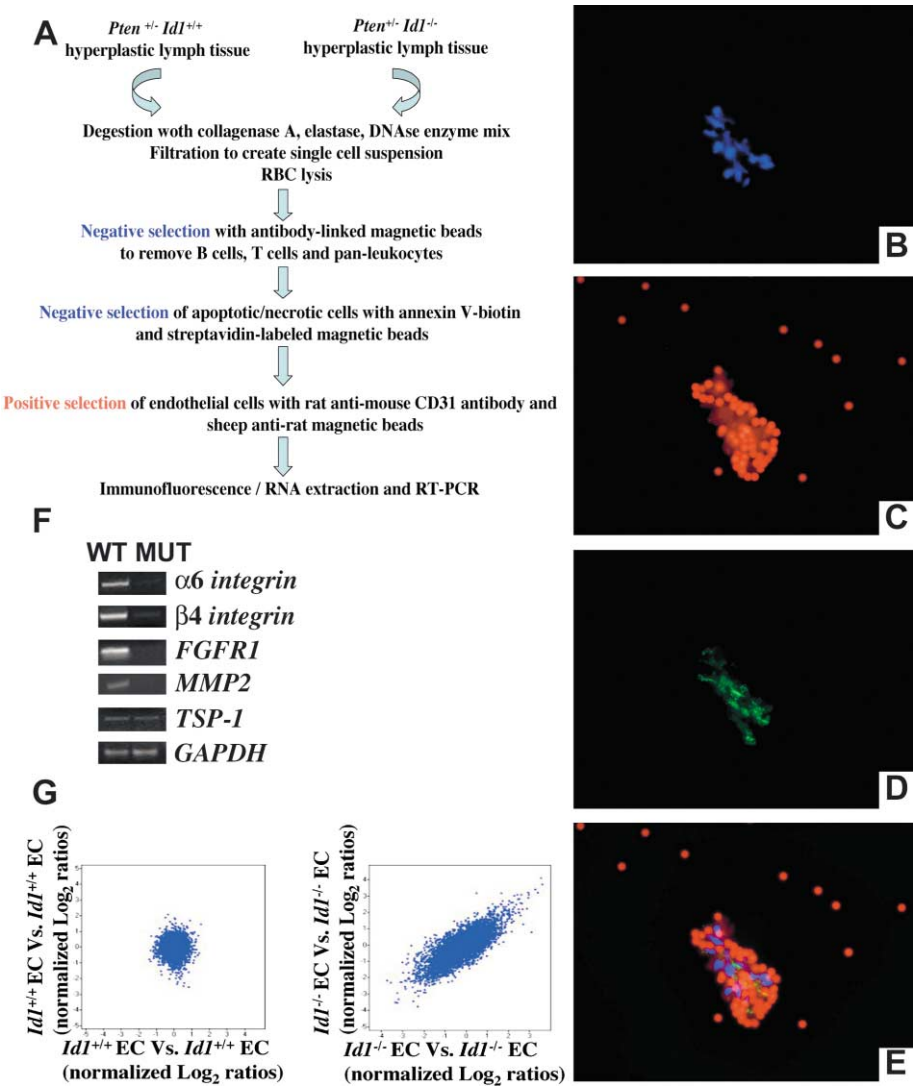

Figure 6. Endothelial cell isolation and analysis

A: Scheme for isolation of pure EC populations from tumors of *Id1*-wild-type and mutant mice.
B–E: Immunofluorescence was used to assess purity of EC preparations. Isolated cells were counted using (**B**) DAPI stain, and their identity confirmed via (**C**) CD31 staining of cell membrane (the beads used to isolate cells are also positive) and (**D**) Von Willebrand factor staining of intracellular Weibel-Palade bodies. (**E**) Merging of images demonstrates that cells express both CD31 and vWF.
F: Semiquantitative RT-PCR confirmed that expression of candidate genes identified in general screen was specifically downregulated in endothelial cells, while expression of *TSP-1* was unchanged.
G: Scatter plot showing normalized Log2 ratios profiles. Comparison of array data from RNA amplified from two independent $Id1^{+/+}$ tumor endothelium samples (left) and from RNA amplified from $Id1^{+/+}$ and $Id1^{-/-}$ tumor endothelium (right).

and, accordingly, we found varying degrees of necrosis and hemorrhage in $Pten^{+/-}$ *Id* mutant tumors lacking functional tumor vasculature. While in the case of lymphocytic hyperplasia, impaired vasculature resulted in pinpoint hemorrhages, uterine carcinoma cells proved to be more susceptible to hypoxia, and very little viable tissue was found in uterine masses grown in *Id* mutant animals. These findings indicate that certain tumors could be more susceptible than others to the effects of antiangiogenic therapy as a single therapeutic modality. Loss of *Id* may make tumors more susceptible to conventional treatment, since increased vascular permeability would result in increased delivery of therapeutic drugs to tumor cells that are already hypoxic, and thus, more susceptible to a "second hit" such as chemotherapy. Indeed, it has been shown recently that loss of *Id* genes synergizes with 17-AAG drug treatment to completely suppress the growth of her2/neu driven mammary carcinomas in mice (de Candia et al., in press).

We prove that *Id1* and *Id3* genes play a crucial role in tumor angiogenesis, since loss of these genes causes vascular defects in both xenografts and the more physiologically relevant genetic tumor models. However, our results also highlight the fact that, under severe angiogenic stress, the behavior of xenografts is often different from that of spontaneously arising tumors. The growth of $Pten^{+/-}$ *Id* mutant lesions differed significantly from the behavior of B6RV2 lymphoma and B-CA breast cancer xenografts, which completely failed to grow when tested in $Id1^{+/-}$ $Id3^{-/-}$ animals (Lyden et al., 1999). Importantly, the vascular phenotype itself differed significantly between xenografts and spontaneously arising tumors in *Id* mutant animals: the angiogenic defect manifested as occluded and stunted vessels in LLC xenografts of *Id* mutant animals (Lyden et al., 1999), whereas in $Pten^{+/-}$ tumors, reduced Id gene expression produced anastamosing and dilated vasculature very similar to that found in the developing neuroepithelium of $Id1^{-/-}Id3^{-/-}$ embryos (Lyden et al., 1999). Thus, our results suggest that xenograft studies provide only limited insight into behavior of spontaneously arising tumors, and genetic tumor models may be more appropriate for testing antiangiogenic agents.

Theories of tumor angiogenesis postulate, based largely on the results of xenograft experiments, that tumors are unable to grow past a few millimeters without a functional neovasculature (Kerbel, 2000). Our results provide evidence that, in physiologi-

Table 1. Genes differentially expressed in Id1$^{-/-}$ versus Id1$^{+/+}$ endothelial cells in lymphoid hyperplasias

Genes downregulated in Id1$^{-/-}$ EC	
Confirmed targets	*α6 integrin (AW556992)*
	β4 integrin (AA407046)
	Fibroblast growth factor receptor 1 (AW557998)
	MMP2 (M84324)
TGFβ/BMP family	*BMP4 (AW537809)*
	TGFβ- induced transcript 4 (AW546174)
IGF family	*IGF 2* (AW538165)
	IGF2 receptor (AW556473)
	IGF binding protein 3 (AW557928)
Ephrins	*Ephrin A1* (AA409240)
	Ephrin receptor A2 (AW545284)
	Ephrin receptor B4 (Z49085)
Cell-cell adhesion	*Protocadherin 13* (AW557174)
	Cadherin 11 (AW555163)
	Junction plakoglobin (AW539609)
	Junction cell adhesion molecule (AW557063)
ECM proteins	*Procollagen, type V, α2* (AW558340)
	Procollagen, type XVIII, α1 (AU042961)
	Laminin α5 (AA408762)
	Laminin γ1 (AW546446)
	Fibronectin 1 (AW547266)
Genes upregulated in Id1$^{-/-}$ EC	
Transcriptional regulation/hypoxia	*Hypoxia-inducible factor 1, alpha subunit* (AW543477)
ECM	*Syndecan-binding protein* (AW537357)
	Chondroitin-sulfate proteoglycan (AW546323)
TGFβ/BMP family	*TGFβ-induced (betaig-h3)* (AW546788)

cal models of tumorigenesis, tumor growth is not entirely prevented under these conditions. The difference in susceptibility to *Id* loss between xenografts and spontaneously arising tumors may lie in the different origins of tumor endothelial cells. In spontaneous tumor angiogenesis, vessels can potentially sprout from co-opted neighboring vasculature or be recruited as BM-derived CEPs (Holash et al., 1999; Rafii, 2000). Previous work has shown that vascularization of xenografts, however, relies mainly on CEPs, mobilization of which is blocked in the *Id*-deficient background. Thus, the less dramatic effect on *Pten*$^{+/-}$ lymph hyperplasia in the *Id* mutant background may be due to co-option of local vasculature in these lesions. Interestingly, even among xenografts, LLC growth, which has a lower contribution of BM-derived precursors, is less affected in *Id* mutant backgrounds than B6RV2, which derives its endothelium almost exclusively from CEPs. In spontaneous tumors, contribution of BM-derived cells to tumor neovessels also differs depending on the tumor type. BM-derived CEPs contributed to 16% of neovessels in *Pten*$^{+/-}$ uterine carcinomas, while CEP contribution to vasculature of lymph hyperplasia was undetectable. Importantly, the effect of *Id* loss was much more profound on the viability of uterine carcinomas than the lymph hyperplasias, which may be due to the dependence on CEPs in the former case and cooption and sprouting of local vessels, less affected by *Id* loss, in the latter. The non-BM-derived vessels formed in the lymph hyperplasia are at least partially dependent on the function of *Id* genes, as vasculature of the *Id*-deficient lymph hyperplasias is morphologically and functionally abnormal. Whether such tumor-specific responses are observed to correlate with CEP utilization and inhibition by other antiangiogenic agents needs to be evaluated.

Using microarray and matrigel assays, we also established that the angiogenic defect in *Id*-deficient mice may be attributed to combined downregulation of MMP-2 and FGFR-1 and α6β4 integrin. α6β4 integrin is expressed in endothelial cells in vivo, but its function has not been established (Kennel et al., 1992). Multiple lines of evidence indicate that MMP-2 is an important regulator of angiogenesis (Haas and Madri, 1999), and downregulation of this molecule in xenografts was previously seen in *Id*-deficient backgrounds (Lyden et al., 1999). FGFR-1 is expressed in endothelial cells as a primary receptor for bFGF, a potent angiogenic growth factor (Nakamura et al., 2001). Previous findings suggest that these angiogenic molecules may lie in the same pathway: bFGF upregulates the expression of α6β4 integrins and MMP-2 activity in endothelial cells in vitro (Klein et al., 1993; Pfeifer et al., 2000), and MMP-2 induces the migration of epithelial cells by cleaving and regulating the function of laminin-5, a recognized ligand for α6β4 integrin (Giannelli et al., 1997). Thus, if the same pathway operated in endothelial cells, loss of *Id* may short-circuit it by downregulation of three of its critical components.

Recently, transcription factor Egr-1 has been implicated in the activation of bFGF, and loss of *Egr-1* produces an antiangiogenic phenotype similar to that of *Id* mutant animals (Fahmy et al., 2003; Lyden et al., 1999, 2001). Interestingly, Egr-1 has also been shown to directly activate *Id1* expression (Tournay and Benezra, 1996). It is possible that the antiangiogenic defect in *Egr-1*-deficient animals is partially due to subsequent downregulation of Id proteins and their targets, bFGF and its receptor.

Microarray analysis carried out on purified endothelial cells also revealed downregulation of other proangiogenic factors, such as members of the ephrin and IGF families, suggesting that Id1 may be regulating several different angiogenic pathways. Ephrin A1 and its receptor EphA2, which are both expressed in xenograft and spontaneous tumor vasculature (Ogawa et al., 2000), have been shown to induce endothelial cell migration

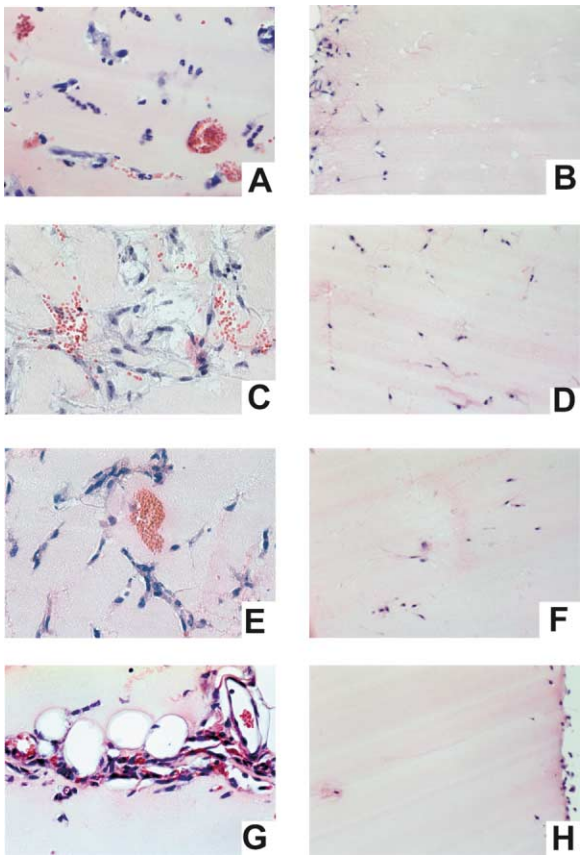

Figure 7. Angiogenic defects associated with blocking downstream targets of Id1 in vivo

A and B: H&E staining of matrigel plugs reveals multiple invading cells arranged in endothelial tubes in (**A**) wild-type animals (n = 10) and no endothelial channels and greatly reduced cell numbers in (**B**) *Id1*$^{-/-}$*Id3*$^{+/-}$ animals (n = 6).

C–H: Inhibition of candidate genes in matrigel assay in vivo. Wild-type mice were implanted with matrigel premixed with (**C**) matched isotype control antibody (n = 3) or (**D**) α6 blocking antibody (n = 10); (**E**) matched isotype control antibody (n = 3) or (**F**) FGFR-1 blocking antibody (n = 10); or (**G**) vehicle alone (n = 3) or (**H**) synthetic peptide with preferential activity against MMP2 (n = 8).

Scale bar, 25 μm (**A**–**H**).

and in vitro capillary assembly as well as corneal and tumor neovascularization (Brantley et al., 2002). EphB4 and its ligand Ephrin B2 are critical in embryonic angiogenesis (Gerety et al., 1999). EphB4 is preferentially expressed on veins, and its activation mediates endothelial cell migration and proliferation in vitro (Gerety et al., 1999; Steinle et al., 2002). IGF2 and its receptor, downregulated in *Id1*$^{-/-}$ endothelial cells, also possess angiogenic properties. IGF 2 induces endothelial cell migration and tube formation, and upregulates expression of MMP-2 (Lee et al., 2000). Thus, downregulation of these factors in the *Id1*$^{-/-}$ endothelial cells may be contributing to the antiangiogenic phenotype of *Id* mutant animals. Future experimental work will be necessary to establish connections between different angiogenic pathways regulated by Id proteins. Interestingly, members of TGFβ/BMP and IGF families have been shown to regulate *Id* gene expression (Ruzinova and Benezra, 2003; Prisco et al., 2001), and our results suggest reciprocal regulation of these factors by *Id*.

Upregulation of *Hif1*α mRNA in the *Id* mutant endothelium suggests a possible direct transcriptional effect, since *Hif1*α promoter has four conserved E box consensus sequences, which are recognized by bHLH transcription factors (Iyer et al., 1998). Unlike upregulation of HIF1α protein in *Id1*$^{-/-}$ tumor cells, this increase is probably not a response to hypoxia, which is mediated via posttranslational stabilization of the HIF1α subunit (Harris, 2002).

While our results confirmed that *TSP-1* is upregulated in *Id* mutant MEFs, our analysis failed to detect similar upregulation in *Pten*$^{+/-}$ *Id1*$^{-/-}$ tumors, suggesting that such a mechanism cannot account for the angiogenesis defect observed in spontaneous tumors of these animals. The observed differences in downstream targets of Id1 are most likely due to the differences between the in vitro system used in the previous report (Volpert et al., 2002) and the in vivo system used in this study, highlighting the importance of using physiologically relevant models.

In this study, we demonstrate that, in the presence of severe antiangiogenic stress, spontaneous tumors in mice can grow beyond a limited size, although this growth is accompanied by extensive hemorrhage and necrosis. Importantly, the extent of tissue damage and the origin of the tumor vasculature is dependent on the tumor type. It is our belief that the mouse models of spontaneous tumors will provide the most useful test of the effectiveness of antiangiogenic therapies alone or in combination with standard chemotherapeutics. Such analysis will be instrumental in realizing the promise of antiangiogenic therapies for the treatment of human cancers.

Experimental procedures

Generation of *Id*-mutant *Pten* mice

Pten$^{+/-}$ and *Id1*$^{-/-}$ *Id3*$^{+/-}$ mice, both in a mixed C57B6/129Sv background, were crossed to generate *Pten*$^{+/-}$ *Id1*$^{+/-}$ *Id3*$^{+/-}$ mice that then were crossed with each other to generate *Pten*$^{+/-}$ mice with intact *Id* copies or *Pten*$^{+/-}$ mice lacking *Id* copies in different combinations. All mice were genotyped by PCR according to previously published protocols (Lyden et al., 1999; DiCristofano et al., 1999) and maintained in compliance with IACUC guidelines.

Histological analysis, immunohistochemistry, and in situ hybridization

Tumor tissue and Matrigel plugs were processed as previously described (Lyden et al., 1999, 2001). Primary antibodies used included antibodies to CD31, α6 integrin (BD Pharmingen, CA), HIF1α (Novus Biologicals, CO), TSP-1, MMP-2 (NeoMarkers, Inc., CA), CD31, Id1, FGFR1, β4 integrin (Santa Cruz Biotechnology, CA), and VEGFR1 and 2 (Imclone Systems Inc., New York, NY). For in situ hybridization, sections were hybridized to [α-^{33}P]UTP labeled antisense RNA probes as described (Jen et al., 1996).

Quantitation of tumor composition and vascular density

Sections from peripheral and central regions of a tumor were imaged at low magnification and areas of tumor tissue, hemorrhage, and necrosis were evaluated using MetaMorph 6.1 program (Universal Imaging Software). 25–35 sections were evaluated per each tumor sample. Blood vessel density was quantified by counting the total number of CD31^{+} vessels across the whole sections of tumors (4–6 sections for each tumor sample).

Semiquantitative assessment of immunohistochemistry intensity

Intensity of staining was estimated using MetaMorph 6.1 (Universal Imaging Software), with intensity scale set to 0% for white and 100% for black. 4–8 images were evaluated for each sample.

Bone marrow transplantation and LacZ detection

Experimental procedures were carried out as previously described (Lyden et al., 2001).

Permeability assay
Vascular permeability assay was performed as previously described (Grunstein et al., 1999).

Tumor samples and RNA extraction
All of the tumor samples were frozen in liquid nitrogen and stored at −80°C. RNA isolation was carried out by using the Invitrogen FastTrack 2.0 mRNA kit (Invitrogen/Life Technologies, CA) and Micro RNA kit (Stratagene, CA). T7-based amplification was carried out by using RiboAmp kit (Arcturus, CA). RNA quality and quantity was assessed via electrophoresis, UV spectrophotometry, or bioanalyzer (Agilent technologies, CA).

cDNA microarrays and data analysis
Conversion of mRNA to double-stranded cDNA was performed by using the superscript cDNA synthesis (Gibco/Life Technologies, CA). Amino-allyl modified dUTP was incorporated into the cDNA. Indirect labeling was accomplished by incubating amino-allyl modified Cy3 or Cy5 dyes (Amersham, NJ). A set of 15,000 sequence-verified mouse cDNA clones representing both known genes and ESTs obtained from National Institute of Aging (http://lgsun.grc.nia.nih.gov/cDNA/15k.html) were PCR amplified, purified, and robotically spotted on glass slides (Stolarov et al., 2001). Arrays were processed and hybridized according to protocols available on our web site (http://nucleus.cshl.org/microarray). After hybridization, the arrays were scanned using a GenePix 4000 laser scanner (Axon Instruments, CA) at 10 μM resolution to measure fluorescence. Raw data files generated by the scanner software GENEPIX3 were imported into S-Plus (a mathematical/statistical package from Insightful Corp, WA) for analysis. For normalization, features for which R^2 values were above 0.4 and 50% feature pixels were 1 standard deviation above background pixels in both channels were considered. The data points were then median normalized and plotted. Experiments were performed in duplicate with color reversals (four hybridizations per sample pair). Each comparison was performed in three different animal pairs. Hierarchical clusters were generated by the Cluster program and visualized with the TreeView program (Eisen et al., 1998) (http://www.microarrays.org/software). We obtained significant correlation (>0.8) in independent hybridizations from samples processed in parallel. To measure the extent of variability for each sample, we performed a self-to-self hybridization, where each sample was labeled with Cy3 or Cy5 and hybridized. In control experiments comparing samples of the same genotype, scatter was minimal, with very few ratios observed to be >0. These were considered noise and were eliminated from the final analysis.

RT-PCR
All RNA samples were treated with DNase I and converted to cDNA using Superscript Single Strand Synthesis kit (Invitrogen/Life Technologies, CA). Primer sequences for *α6* and *β4 integrins* (Zent et al., 2001), *MMP-2* (Kanwar et al., 1999), *TSP-1* (Volpert et al., 2002), *FGFR-1*, and *GAPDH* (Faloon et al., 2000) have been previously published. All RT-PCRs were performed within dynamic range.

Endothelial cell isolation
Tumor tissue was incubated for 1 hr with collagenase A, elastase, and DNaseI (Roche, Germany) and then filtered to produce single cell suspension. Erythrocytes were removed using RBC Lysis Buffer (Roche, Germany). Negative selection was performed by incubating cell suspension with pan B- and pan T-magnetic beads (Dynal Biotech ASA, Norway) as well as magnetic beads (Dynal Biotech ASA) prelabeled with pan-leukocytic CD45 antibody (BD Pharmingen, CA). Dead cells were removed by incubation with Annexin V-biotin (Roche,Germany) and then streptavidin magnetic beads (Dynal Biotech ASA, Norway). Endothelial cells were selected by labeling with CD31 antibody (BD Pharmingen, CA) and incubation with magnetic beads (Dynal Biotech ASA, Norway).

Immunofluorescence
Cells were fixed in 4% paraformaldehyde and stained with antibodies to CD31 (BD Pharmingen, CA) and Von Willebrand factor (DAKO A/S, Denmark). Secondary staining used Alexa 488 and Alexa 546 conjugated antibodies (Molecular Probes, Inc. Oregon). DNA was visualized with DAPI.

Matrigel assay
Assays were carried out as previously described (Lyden et al., 2001). Matrigel plugs were also impregnated with: α6 blocking antibody, matched isotype antibodies (BD Pharmingen, CA), MMP-2 inhibiting peptide (Oncogene Research Products, San Diego, CA), and FGFR-1 blocking antibody (Chemicon International, Temecula, CA) at previously published concentrations (Zent et al., 2001; Meitinger et al., 2001; Koivunen et al., 1999).

Statistical analysis
Student's t test was used to determine statistical significance between experimental groups. $P < 0.05$ was considered significant and is indicated with an asterisk over the value in Figures 1 and 2. P values of <0.01 and 0.001 are indicated by double and triple asterisks, respectively.

Supplemental data
All Supplemental Figures can be found at http://www.cancercell.org/cgi/content/full/4/4/277/DC1.

Acknowledgments

We thank the staff of the MSKCC Molecular Core Facility and the CSH microarray shared resource for their technical assistance. This research was supported by NIH MSTP grant GM07739 (to M.B.R.) and grants from NIH and Angiogenex (to R.B.).

Received: June 2, 2003
Revised: August 27, 2003
Published: October 20, 2003

References

Bergers, G., Javaherian, K., Lo, K.M., Folkman, J., and Hanahan, D. (1999). Effects of angiogenesis inhibitors on multistage carcinogenesis in mice. Science *284*, 808–812.

Brantley, D.M., Cheng, N., Thompson, E.J., Lin, Q., Brekken, R.A., Thorpe, P.E., Muraoka, R.S., Cerretti, D.P., Pozzi, A., Jackson, D., et al. (2002). Soluble Eph A receptors inhibit tumor angiogenesis and progression in vivo. Oncogene *21*, 7011–7026.

Carmeliet, P., and Jain, R. (2000). Angiogenesis in cancer and other diseases. Nature *407*, 249–257.

de Candia, P., Solit, D.B., Giri, D., Brogi, E., Siegel, P.M., Olshen, A.B., Muller, W., Rosen, N., and Benezra, R. (2003). Angiogenesis impairment in Id deficient mice cooperates with the HSP90 inhibitor 17-AAG to completely suppress her2/neu dependent breast tumors. Proc. Natl. Acad. Sci. USA, in press.

Di Cristofano, A., Kotsi, P., Peng, Y.F., Cordon-Cardo, C., Elkon, K.B., and Pandolfi, P.P. (1999). Impaired Fas response and autoimmunity in Pten+/− mice. Science *285*, 323–334.

Di Cristofano, A., De Acetis, M., Koff, A., Cordon-Cardo, C., and Pandolfi, P.P. (2001). Pten and p27KIP1 cooperate in prostate cancer tumor suppression in the mouse. Nat. Genet. *27*, 222–224.

Eisen, M.B., Spellman, P.T., Brown, P.O., and Botstein, D. (1998). Cluster analysis and display of genome-wide expression patterns. Proc. Natl. Acad. Sci. USA *95*, 14863–14868.

Fahmy, R.G., Dass, C.R., Sun, L.Q., Chesterman, C.N., and Khachigian, L.M. (2003). Transcription factor Egr-1 supports FGF-dependent angiogenesis during neovascularization and tumor growth. Nat. Med. *9*, 1026–1032.

Faloon, P., Arentson, E., Kazarov, A., Deng, C.X., Porcher, C., Orkin, S., and Choi, K. (2000). Basic fibroblast growth factor positively regulates hematopoietic development. Development *127*, 1931–1941.

Gerety, S.S., Wang, H.U., Chen, Z.F., and Anderson, D.J. (1999). Symmetrical mutant phenotypes of the receptor EphB4 and its specific transmembrane ligand ephrin-B2 in cardiovascular development. Mol. Cell *4*, 403–414.

Giannelli, G., Falk-Marziller, J., Shiraldi, O., Stetler-Stevenson, W., and Quar-

anta, V. (1997). Induction of Cell Migration by Matrix Metaloprotease-2 Cleavage of Laminin-5. Science *277*, 225–227.

Grunstein, J., Roberts, W.G., Mathieu-Costello, O., Hanahan, D., and Johnson, R.S. (1999). Tumor-derived expression of vascular endothelial factor is a critical factor in tumor expansion and vascular function. Cancer Res. *59*, 1592–1598.

Haas, T.L., and Madri, J.A. (1999). Extracellular matrix-driven matrix metalloproteinase production in endothelial cells: implications for angiogenesis. Trends Cardiovasc. Med. *9*, 70–77.

Harris, A.L. (2002). Hypoxia – a key regulatory factor in tumor growth. Nat. Rev. Cancer *2*, 38–47.

Holash, J., Maisonpierre, P.C., Compton, D., Boland, P., Alexander, C.R., Zagzag, D., Yancopoulos, G.D., and Wiegand, S.J. (1999). Vessel cooption, regression, and growth in tumors mediated by angiopoietins and VEGF. Science *284*, 1994–1998.

Iyer, V.I., Leung, S.W., and Semenza, G.L. (1998). The human hypoxia-inducible factors 1α gene: *HIF1*α structure and evolutionary conservation. Genomics *52*, 159–165.

Jen, Y., Manova, K., and Benezra, R. (1996). Expression patterns of Id1, Id2, and Id3 are highly related but distinct from that of Id4 during mouse embryogenesis. Dev. Dyn. *207*, 235–252.

Kanwar, Y.S., Ota, K., Yang, Q., Wada, J., Kashihara, N., Tian, Y., and Wallner, E.I. (1999). Role of membrane-type matrix metalloproteinase 1 (MT-1-MMP), MMP-2, and its inhibitor in nephrogenesis. Am. J. Physiol. *277*, 934–947.

Kennel, S.J., Godfrey, V., Ch'ang, L.Y., Lankford, T.K., Foote, L.J., and Makkinje, A. (1992). The beta 4 subunit of the integrin family is displayed on a restricted subset of endothelium in mice. J. Cell Biol. *101*, 145–150.

Kerbel, R.S. (2000). Tumor angiogenesis: past, present and near future. Carcinogenesis *21*, 505–515.

Klein, S., Giancotti, F.G., Presta, M., Albelda, S.M., Buck, C.A., and Rifkin, D.B. (1993). Basic fibroblast growth factor modulates integrin expression in microvascular endothelial cells. Mol. Biol. Cell *4*, 973–982.

Koivunen, E., Arap, W., Valtanen, H., Rainisalo, A., Medina, O.P., Heikkila, P., Kantor, C., Gahmberg, C.G., Salo, T., Konttinen, Y.T., et al. (1999). Tumor targeting with a selective gelatinase inhibitor. Nature Biotechnol. *17*, 768–774.

Lee, O.H., Bae, S.K., Bae, M.H., Lee, Y.M., Moon, E.J., Cha, H.J., Kwon, Y.G., and Kim, K.W. (2000). Identification of angiogenic properties of insulin-like growth factor II in in vitro angiogenesis models. Br. J. Cancer *82*, 385–391.

Lyden, D., Young, A.Z., Zagzag, D., Yan, W., Gerald, W., O'Reilly, R., Bader, B.L., Hynes, R.O., Zhuang, Y., Manova, K., and Benezra, R. (1999). Id1 and Id3 are required for neurogenesis, angiogenesis and vascularization of tumour xenografts. Nature *401*, 670–677.

Lyden, D., Hattori, K., Dias, S., Costa, C., Blaikie, P., Butros, L., Chadburn, A., Heissig, B., Marks, W., Witte, L., et al. (2001). Impaired recruitment of bone-marrow-derived endothelial and hematopoietic precursor cells blocks tumor angiogenesis and growth. Nat. Med. *7*, 1194–1201.

Meitinger, D., Hunt, M., Shih, D.T., Fox, J.C., and Hunt, R.C. (2001). Vitreous-induced modulation of integrins in retinal pigment epithelial cells: effects if fibroblast growth factor-2. Exp. Eye Res. *73*, 681–692.

Nakamura, T., Mochizuki, Y., Kanetake, H., and Kanda, S. (2001). Signals via FGF receptor 2 regulate migration of endothelial cells. Biochem. Biophys. Res. Commun. *289*, 801–806.

Ogawa, K., Pasqualini, R., Lindberg, R.A., Kain, R., Freeman, A.L., and Pasquale, E.B. (2000). The ephrin-A1 ligand and its receptor, EphA2, are expressed during tumor neovascularization. Oncogene *19*, 6043–6052.

Pfeifer, A., Kessler, T., Silletti, S., Cheresh, D.A., and Verma, I.M. (2000). Suppression of angiogenesis by lentiviral delivery of PEX, a noncatalytic fragment of matrix metalloproteinase 2. Proc. Natl. Acad. Sci. USA *97*, 12227–12232.

Powers, C.J., McLeskey, S.W., and Wellstein, A. (2000). Fibroblast growth factors, their receptors and signaling. Endocr. Relat. Cancer *7*, 165–197.

Prisco, M., Peruzzi, F., Belletti, B., and Baserga, R. (2001). Regulation of Id gene expression by type I insulin-like growth factor: roles of Stat3 and the tyrosine 950 residue of the receptor. Mol. Cell. Biol. *21*, 5447–5458.

Rafii, S. (2000). Circulating endothelial precursors: mystery, reality, and promise. J. Clin. Invest. *105*, 17–19.

Ruzinova, M.B., and Benezra, R. (2003). Id proteins in development, cell cycle and cancer. Trends Cell Biol. *13*, 410–418.

St Croix, B., Rago, C., Velculescu, V., Traverso, G., Romans, K.E., Montgomery, E., Lal, A., Riggins, G.J., Lengauer, C., Vogelstein, B., and Kinzler, K.W. (2000). Genes expressed in human tumor endothelium. Science *289*, 1197–1202.

Steinle, J.J., Meininger, C.J., Forough, R., Wu, G., Wu, M.H., and Granger, H.J. (2002). Eph B4 receptor signaling mediates endothelial cell migration and proliferation via the phosphatidylinositol 3-kinase pathway. J. Biol. Chem. *277*, 43830–43835.

Stolarov, J., Chang, K., Reiner, A., Rodgers, L., Hannon, G.J., Wigler, M.H., and Mittal, V. (2001). Design of a retroviral-mediated ecdysone-inducible system and its application to the expression profiling of the PTEN tumor suppressor. Proc. Natl. Acad. Sci. USA *98*, 13043–13048.

Tournay, O., and Benezra, R. (1996). Transcription of the dominant negative helix-loop-helix protein Id1 is regulated by a protein complex containing the immediate early response gene *Egr-1*. Mol. Cell. Biol. *16*, 2418–2430.

Vandeputte, D.A., Troost, D., Leenstra, S., Ijlst-Keizers, H., Ramkema, M., Bosch, D.A., Baas, F., Das, N.K., and Aronica, E. (2002). Expression and distribution of id helix-loop-helix proteins in human astrocytic tumors. Glia *38*, 329–338.

Volpert, O., Pili, R., Sikder, H., Nelius, T., Zaichuk, T., Morris, C., Shifflet, C., Devlin, M., Conant, K., and Alani, R. (2002). Id1 regulates angiogenesis through transcriptional repression of thrombospondin-1. Cancer Cell *2*, 473–483.

Zent, R., Bush, K.T., Pohl, M.L., Quaranta, V., Koshikawa, N., Wang, Z., Kreidberg, J.A., Sakurai, H., Stuart, R.O., and Nigam, S.K. (2001). Involvement of laminin binding integrins and laminin-5 in branching morphogenesis of the ureteric bud during kidney development. Dev. Biol. *238*, 289–302.